Introduction

In the last 100 years the neuroscientific research has been transformed. After the invention of electroencephalogram (EEG) from Berger in 1929 (Berger, 1929) it became apparent that neural activity can be recorded and evaluated. Initially, studies relied on univariate (i.e. single time series) analysis of the brain dynamics. This started to change towards the end of the 20th century with the first functional connectivity (FC) studies (Friston et al., 1993; Biswal et al., 1995). According to this new field, the different brain regions are not isolated islands of brain function; on the contrary they are part of a complex archipelago with extensive interconnections. In more mathematical terms, the brain regions are considered nodes on a graph, interconnected by edges (Rubinov and Sporns, 2010). These edges are defined by the statistical relationship of the neuronal time series under investigation.

Several different FC estimators had been introduced. Pearson's correlation (r_P) was the first estimator applied in FC studies (Friston et al., 1993; Biswal et al., 1995). Some drawbacks of the method (e.g. inability to capture nonlinear dynamics) lead to the introduction of newer methodologies such as phase lag index (PLI) (Stam et al., 2007), synchronization likelihood (SL) (Stam and Van Dijk, 2002) and mutual information (MI) (Steuer et al., 2002; van den Heuvel and Fornito, 2014). The use of different FC estimators can greatly influence the architecture of the constructed networks (Lindquist, 2020; Mukli et al., 2021; Stylianou et al., 2021a). Such inconsistencies have been shown in non-healthy population as well, e.g. in Alzheimer's disease patients (Jalili, 2016). It is then important that a conscious choice should be made before selecting one of the aforementioned (or many other) methods. r_P is still widely used (Demirtaş et al., 2016; Chettouf et al., 2022) due to its simplicity and interpretability. An important advantage of r_P is the capacity to separate positive from negative correlations, something not possible PLI, SL or MI. Yet, r_P was not designed for nonstationary time series.

Signals can be divided in two categories: *i*) stationary and *ii*) nonstationary, based on their variability during time. A mathematical distinction between stationary and nonstationary time series can be made by examining their statistical properties like mean and variance. In stationary signals such properties remain constant, while they vary in nonstationary signals. **Figure 1** shows an exemplary case of these two categories. Most physiological time series are nonstationary due to extrinsic and/or intrinsic perturbations injected into the system. As a result, calculating the variance (and covariance) – integral part of r_P calculation[1] – of the entire signal can be misleading.

[1] r_P between two signals X and Y is: $r_P = \frac{cov_{X,Y}}{\sqrt{var_X var_Y}}$,

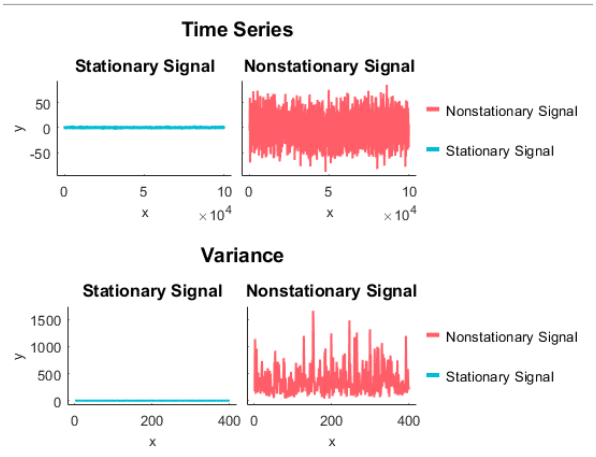

A solution to this issue was given with the introduction of detrended cross-correlation coefficient (DCCC) (Zebende, 2011). DCCC is the average of variance and covariance of smaller sections of the signals (see **Methods**). In this paper we propose an extension of DCCC termed multiscale detrended cross-correlation coefficient (MDC_3). The main advantage of MDC_3 compared to DCCC is the easier interpretability of the results. To show this, we compared MDC_3 to r_P using simulated time series with known coupling. We also demonstrated the differences between the two estimators in EEG and magnetoencephalogram (MEG) recordings.

Methods

Multiscale Detrended Cross-Correlation Coefficient

Before introducing MDC_3 we should explain the detrended cross-correlation coefficient, onto which MDC_3 is based on. DCCC was introduced by Zebende in an attempt to creating a more accurate coupling estimator between nonstationary time series (Zebende, 2011). DCCC is calculated for several scales (s) (or window lengths) as follows. For every scale the two signals X and Y are divided into N non-overlapping windows of s. In every window the linear trend is removed, the detrended signals are denoted by: $\widehat{\ }$. Detrending of time series prior to the investigation of their interconnectivity gives more accurate estimates, since it can (at least partly) counteract any spurious coupling emerging due to autocorrelation effects (Horvatic et al., 2011). Then the average covariance between the two signals and average variances of the two signals are estimated. Finally, the ratio of average covariance and square root of the product of average variances is calculated. **Equation 1** provides a mathematical formula of these steps.

$$DCCC(s) = \frac{\frac{1}{N}\sum_{i=1}^{N} cov_{\widehat{X},i,\widehat{Y},i}}{\sqrt{\frac{1}{N}\sum_{i=1}^{N} var_{\widehat{X},i}\ \frac{1}{N}\sum_{i=1}^{N} var_{\widehat{Y},i}}}$$

DCCC is reminiscent of r_P since both estimators range between -1 and 1 with negative values corresponding to anticorrelation and positive values corresponding to correlation (Podobnik et al., 2011). Yet, DCCC is a more accurate estimator, especially in the case of

nonstationary signals (Kristoufek, 2014). It seems then that DCCC is a valid replacement of r_P, yet the use of a multitude of scales can be hard to interpret. For example, assume that we calculate the DCCC between *X* and *Y* using the following scales s = [50, 100, 150, 200, 250, 300] and end up with the following values: [0.3, 0.6, 0.1, -0.3, 0.02, -0.1]. Are the two signals correlated or anticorrelated and in what extent? It is not possible to draw a clear conclusion. We believe that MDC_3 could offer a mathematically sound solution to this problem.

The estimation of MDC_3 starts by calculating DCCC for different scales. To avoid any arbitrary choice of scales, MDC_3 uses a series of frequencies (*f*) which can be converted to scales when the sampling rate (*SR*) is known ($s=SR/f$). After the estimation of DCCC for every frequency, the cross-spectral density of each pair of detrended time series[2] is estimated and the relative power of the used frequencies is found. Based on this relative power, we calculate the weighted average of DCCC. The distribution of DCCC behaves similarly to r_P's distribution, so before the calculation of the weighted average DCCC is normalized using Fisher's *z* transform (Alexander, 1990; Corey et al., 1998). Details about MDC_3 can be found in the pseudo-code in **Table 1**.

INPUTS: time series X; time series Y; minimum frequency; maximum frequency; frequency step; sampling rate; detrending degree
frequencies = ([minimum frequency, maximum frequency], increment = frequency step)
scales = sampling rate / frequencies
for every scale
  for every window
    detrend (window of time series X, window of time series Y, degree = detrending degree)
    covariance_XY (window of time series X, window of time series Y)
    variance_X (window of time series X)
    variance_Y (window of time series Y)
  dccc = mean (covariance_XY) / sqrt([mean (variance_X)*mean (variance_Y)])
detrend (time series X, time series Y, degree = detrending degree)
cross-spectral density (detrended X, detrended Y)
weights = frequency specific cross-spectral power / total cross-spectral power
mdc3 = tanh {sum [$\tanh^{-1}$ (dccc)*weights]}
OUTPUT: mdc3

Simulated Time Series

[2] In this case the whole signals are detrended.

In order to validate the efficacy of MDC_3 we simulated pairs of fractionally auto-regressive integrated moving-average (ARFIMA) processes with known cross-correlation, as in Kristoufek (Kristoufek, 2014). These series are calculated as follows:

$$A = \sum_{n=0}^{100} \alpha_n(d)\varepsilon_{A,t-n}$$

$$B = \sum_{n=0}^{100} \alpha_n(d)\varepsilon_{B,t-n}$$

ε_A is sampled from a standard normal distribution. In order to inject cross-correlation ρ between the two time series $\varepsilon_B = \rho\varepsilon_A + \varepsilon\sqrt{1-\rho^2}$, with ε being sampled from a standard normal distribution. $\alpha_n(d) = \frac{\Gamma(n+d)}{\Gamma(n+1)\Gamma(d)}$, where Γ is the gamma function. The parameter d defines the nonstationary of the simulated signal; $d < 0.5$ corresponds to stationary time series, $d \geq 0.5$ corresponds to nonstationary time series. The greater the d, the more nonstationary the signal is going to be.

Kommentiert [OS1]: Do you think I should add the proof in an appendix? I just start with cov(A,B) and after simplifications I end up with ρ.

We wanted to study the effect on the whole range of coupling for both stationary and nonstationary time series. So we employed the same parameters as Kristoufek (Kristoufek, 2014): *i*) $d = [0.1,1.4]$ with increments of 0.1and *ii*) $\rho = [-0.,0.9]$ with increments of 0.1. We wanted to demonstrate the benefits of MDC_3 in real-life neuronal time series, hence our simulations consisted of two types. The first type were signals trying to emulate EEG/MEG signals with an assumed sampling rate of 250 Hz and three different lengths: 1000, 5000 & 10000 datapoints, corresponding to 4, 20 and 40 seconds of recordings. The frequency range of MDC_3 was from 0.5 to 31.25 Hz with increments of 0.5. In the second type we wanted to study how lower sampling rates, seen in fMRI, will affect our methodology. As a result, the second type had an assumed sampling rate of 1 Hz and lengths of 100, 200 & 500 datapoints (i.e. 100, 200 and 500 seconds). The frequency range of MDC_3 was from 0.01 to 0.125 Hz with increments of 0.01. In both types, the maximal frequencies were selected so there were at least 8 datapoints in every window for covariance and variance calculation. We run 1000 simulations for each model.

We wanted to see how closely to the real coupling the two estimators (MDC_3 and r_P) are. We calculated the mean squared error for every ρ, d and signal length. Then, simulations of the same ρ were group together. As a result, we ended up with 84 (6 signal lengths x 14 d) pairs of 19-points (19 ρ) distributions. We performed a one-sided Wilcoxon rank sum test (α=0.05) for every pair. Finally, Benjamini-Hochberg (Benjamini and Hochberg, 1995) correction was used to counteract the effect of multiple comparisons.

Neuronal Time Series

We also wanted to show how misleading r_P could be in neuronal time series. For demonstrating purposes, we analyzed the following EEG and MEG datasets.

EEG Dataset

The analyzed EEG dataset was made publicly available by George et al. (George et al., 2013). The subject cohort consisted of 15 Parkinson disease (PD) patients (8 females, aged 62.6 ± 8.3 years) and 16 matched healthy control individuals (HC) (9 females, aged 63.5 ± 9.6 years). PD participants were under dopaminergic treatment for which they were responsive. EEG measurements of 3 minutes of eyes open state were taken for the HC group. The PD patients had to perform the study twice, once while being on medication (PD-ON) and once being off medication (PD-OFF) for 12 hours or more. The EEG recording device had 32 channels (according to 10-10 system) and a sampling rate of 512 Hz. All participants provided informed consent. Details about the participants can be found in (George et al., 2013) (Table 1 and Table 2).

The EEG data were visually inspected using EDFbrowser and 8 continuous seconds of artifact-free signal were selected. These segments were transformed to reference-free current source density (CSD) estimated using the spherical spline algorithm (Perrin et al., 1989) as implemented in the CSD toolbox (Kayser and Tenke, 2006a, 2006b); thus spurious interdependencies due to volume conduction effects were minimized. Then, the data were band-pass filtered with lower and upper cutoff frequencies at 0.5 and 45 Hz, respectively, using a Finite Impulse Response filter in EEGLAB toolbox (Delorme and Makeig, 2004). Subsequently, we performed manual independent component analysis (via EEGLAB) (Makeig et al., 1997) in order to remove artifacts (i.e. signal components of extra-neural origin) induced by skeletal muscle activity, cardiac activity, eye movements or blinking. The frequencies used in MDC_3 ranged from 0.5 to 45 Hz with increments of 0.5. Second degree polynomials were fitted for the detrending. Finally, we estimated the FC between different brain regions using r_P as well.

MEG Dataset

Gianluca's work

Results

Simulated Time Series

As shown in **Figure 2** MDC_3 is a more accurate estimator of coupling in the simulated signals in almost every case. Exceptions are the cases of d = [0.1,0.2] where no difference was observed between the two estimators, in any signal length. Only some small difference can be observed for stationary signals (d = [0.3,0.4]); but as we transition to nonstationary time series (d >0.5), the inability of r_P to estimate real coupling is apparent. We also see that MDC_3 is more accurate for shorter time series. Additional figures from the simulations can be found in the **supplementary material**.

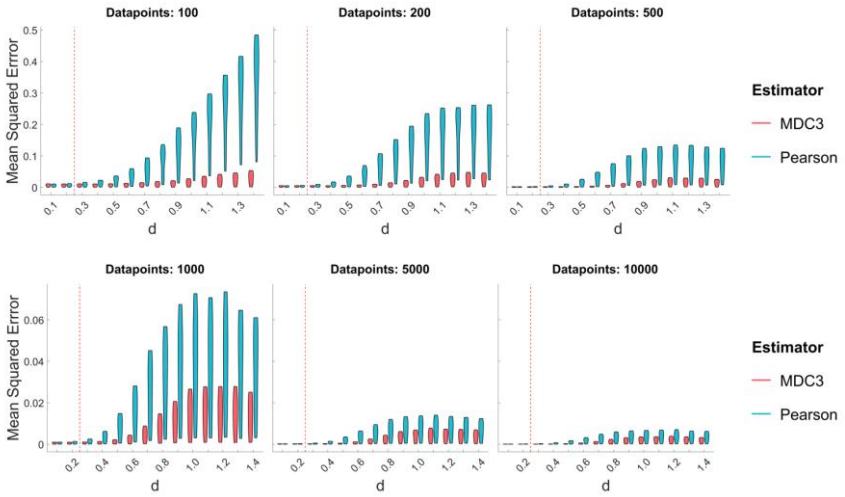

Neuronal Time Series

Figure 3 shows exemplary cases of the difference of FC matrices calculated using MDC_3 and r_P. A substantial number of the estimated values does not seem to correspond between the two FC estimators, with some cases the difference being higher than 0.4. Such disagreements were apparent in all groups (HC, PD-ON & PD-OFF). The complete list of figures for every participant can be found in the **supplementary material**.

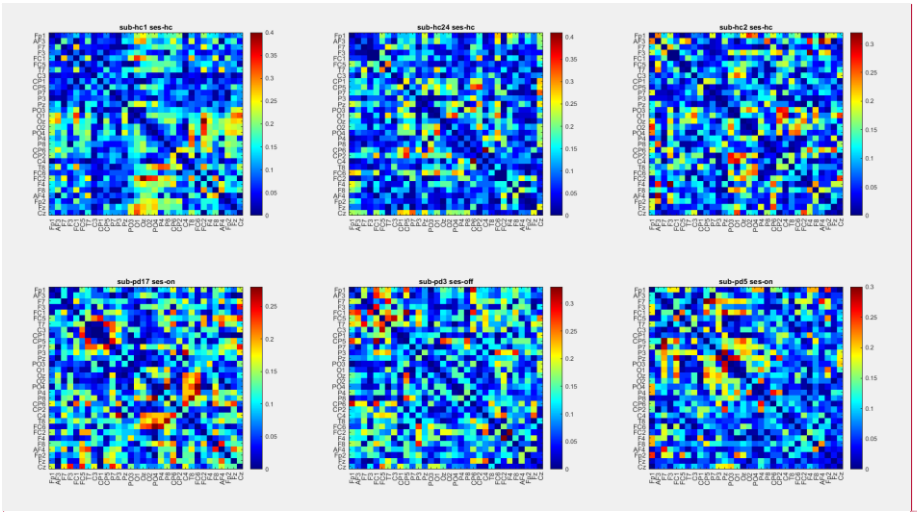

Kommentiert [OS2]: This is absolute difference

+ MEG data

Discussion

In this study we introduced MDC_3, an extension of DCCC; its advantage over the original DCCC is that by taking a weighted average of the DCCC for each scale we obtain a single value for every connection. Our simulations with signals of known coupling showed that MDC_3 is a more accurate FC estimator than r_P. The exemplary FC analysis of EEG and MEG data also showed that the use of MDC_3 could lead to major differences in the connectivity matrices compared to r_P.

We simulated 1000 pairs time series for different coupling strengths, signal lengths and nonstationarity cases. For every pair we calculated MDC_3 and r_P. As explained in the **Introduction**, and shown in **Figure 1**, the variance of stationary signals remains constant. Hence, the average of variances (used for DCCC) and whole variances (used for r_P) will be similar. This is not the case for nonstationary series whose variance heavily depends on time. Our simulations support this since the MSE of MDC_3 was significantly smaller in every case, except for fairly stationary signals (**Figure 2**). The discrepancy between the two estimators increased greatly in higher nonstationarity. Similar findings have been reported for DCCC in Kristoufek (Kristoufek, 2014). Another finding agreeing with Kristoufek (Kristoufek, 2014) is that the higher the signal length the less accurate MDC_3 is going to be. A potential solution could be the inclusion of lower frequencies. In our simulations the lower cutoffs were 0.5 and 0.01 Hz, frequencies that correspond to the lower ranges of brain imaging modalities we wanted to simulate (EEG/MEG and fMRI respectively). Nonetheless, even in longer signals MDC3 was more accurate. The longest signals corresponded to 40 (for EEG/MEG) and 500 (for fMRI) seconds. These epochs are longer than the usual length of epochs studied in neuroscience, at the same time MDC_3 remained superior to r_P.

Of course, statistical significance in simulations without real-life benefits would not warrant the use of MDC_3. To demonstrate its advantages, we used an EEG and MEG dataset, containing both healthy and PD subjects. In both cases, we showed that the FC matrices calculated using MDC_3 could capture substantial differences compared to r_P networks (**Figure 3**). At a first glance someone might be dismissive of this, since it is well known that different estimators can lead to different FC matrices (Mukli et al., 2021; Stylianou et al., 2021a). This would have been the case, if we haven't explained the higher reliability of MDC_3 both from a mathematical standpoint (**Methods**) and simulations (**Results**). We then suggest that FC studies should use MDC_3 over r_P in any case. Even if MDC_3 is computational more intensive, the modern-day computational capabilities make the time difference inconsequential. Finally, it should be noted that MDC_3 is still a linear FC estimator. Nonlinear estimators like MI, PLI and SL still capture dynamics that MDC_3 cannot. In spite of that, we believe that MDC_3 is a valuable addition to the FC field due to its ability to capture the sign of correlation. A common practice in FC studies is the exclusion of negative correlations (Rubinov and Sporns, 2010), hence ability of capturing anticorrelation was not a concern of the field. The human brain operates with several negative feedback loops, powered mainly by GABA-producing interneurons. It is then necessary to study negative connectivity to obtain accurate brain networks, as suggested by previous studies (Chen et al., 2011; Zhan et al., 2017).

DCCC and its extension to MDC_3 are closely related to scale-free analysis of signals. The numerator and denominator of **Equation 1** are in essence the ratio of detrended fluctuation analysis (Peng et al., 1994) and detrend cross-correlation analysis (Podobnik and Stanley, 2008) values, respectively. DCCC has been incorporated in surrogate testing of scale-free coupling already (Podobnik et al., 2011; Blythe et al., 2016; Stylianou et al., 2021a). The main

difference between MDC_3 and DCCC is the output of a single correlation value for the whole signal, as opposed to scale-specific correlations; it is then clear that MDC_3 cannot be used in scale-free analysis. DCCC has also been employed in multifractal analysis of neuronal coupling (Stylianou et al., 2021a, 2021b) and it has already been extended to the multifractal setting (Kwapień et al., 2015); where different exponents capture different size of fluctuations. Theoretically, a multifractal MDC_3 could be created as well. This is beyond the scope of the current study since we focused on improving the interpretability of DCCC. The calculation of MDC_3 using different scaling exponents would add another layer of complexity in the interpretation of the outputs. Recently, a real-time algorithm for the estimation of DCCC was presented (Kaposzta et al., 2022), which can be extended to include MDC_3. This means that MDC_3 can be used in brain computer interfaces or clinical monitoring of patients, where constant tracking of network dynamics is needed.

Conclusion

We presented a new estimator of coupling between time series. Using simulated data, we showed its superiority over r_P. The differences between the two estimators were made apparent in EEG and MEG datasets of healthy and diseased population. Even if our exemplary cases consisted only of neuronal time series, MDC_3 could be used in any time series as long as the sampling rate is known.

Alexander, R. A. (1990). A note on averaging correlations. *Bull. Psychon. Soc.* 28, 335–336. doi:10.3758/BF03334037.

Benjamini, Y., and Hochberg, Y. (1995). Controlling the False Discovery Rate: A Practical and Powerful Approach to Multiple Testing. *J. R. Stat. Soc. Ser. B* 57, 289–300. doi:10.1111/j.2517-6161.1995.tb02031.x.

Berger, H. (1929). Uber das Elektrenkephalogramm des Menschen (On the human electroencephalogram). *Arch. f. Psychiatr. u. Nervenkrankheiten* 87, 527–570. doi:10.1007/BF01797193.

Biswal, B., Zerrin Yetkin, F., Haughton, V. M., and Hyde, J. S. (1995). Functional connectivity in the motor cortex of resting human brain using echo-planar mri. *Magn. Reson. Med.* 34, 537–541. doi:10.1002/mrm.1910340409.

Blythe, D. A. J., Nikulin, V. V., and Müller, K.-R. (2016). Robust Statistical Detection of Power-Law Cross-Correlation. *Sci. Rep.* 6, 27089. doi:10.1038/srep27089.

Chen, G. G., Chen, G. G., Xie, C., and Li, S.-J. J. (2011). Negative Functional Connectivity and Its Dependence on the Shortest Path Length of Positive Network in the Resting-State Human Brain. *Brain Connect.* 1, 195–206. doi:10.1089/brain.2011.0025.

Chettouf, S., Triebkorn, P., Daffertshofer, A., and Ritter, P. (2022). Unimanual sensorimotor learning—A simultaneous <scp>EEG-fMRI</scp> aging study. *Hum. Brain Mapp.*, 1–17. doi:10.1002/hbm.25791.

Corey, D. M., Dunlap, W. P., and Burke, M. J. (1998). Averaging correlations: Expected values and bias in combined pearson rs and fisher's z transformations. *J. Gen. Psychol.* 125, 245–261. doi:10.1080/00221309809595548.

Delorme, A., and Makeig, S. (2004). EEGLAB: an open source toolbox for analysis of single-

trial EEG dynamics including independent component analysis. *J. Neurosci. Methods* 134, 9–21. doi:10.1016/j.jneumeth.2003.10.009.

Demirtaş, M., Tornador, C., Falcón, C., López-Solà, M., Hernández-Ribas, R., Pujol, J., et al. (2016). Dynamic functional connectivity reveals altered variability in functional connectivity among patients with major depressive disorder. *Hum. Brain Mapp.* 37, 2918–2930. doi:10.1002/hbm.23215.

Friston, K. J., Frith, C. D., Liddle, P. F., and Frackowiak, R. S. J. (1993). Functional Connectivity: The Principal-Component Analysis of Large (PET) Data Sets. *J. Cereb. Blood Flow Metab.* 13, 5–14. doi:10.1038/jcbfm.1993.4.

George, J. S., Strunk, J., Mak-McCully, R., Houser, M., Poizner, H., and Aron, A. R. (2013). Dopaminergic therapy in Parkinson's disease decreases cortical beta band coherence in the resting state and increases cortical beta band power during executive control. *NeuroImage Clin.* 3, 261–270. doi:10.1016/j.nicl.2013.07.013.

Horvatic, D., Stanley, H. E., and Podobnik, B. (2011). Detrended cross-correlation analysis for non-stationary time series with periodic trends. *EPL (Europhysics Lett.* 94, 18007. doi:10.1209/0295-5075/94/18007.

Jalili, M. (2016). Functional Brain Networks: Does the Choice of Dependency Estimator and Binarization Method Matter? *Sci. Rep.* 6, 29780. doi:10.1038/srep29780.

Kaposzta, Z., Czoch, A., Stylianou, O., Kim, K., Mukli, P., Eke, A., et al. (2022). Real-Time Algorithm for Detrended Cross-Correlation Analysis of Long-Range Coupled Processes. *Front. Physiol.* 13. doi:10.3389/fphys.2022.817268.

Kayser, J., and Tenke, C. E. (2006a). Principal components analysis of Laplacian waveforms as a generic method for identifying ERP generator patterns: I. Evaluation with auditory oddball tasks. *Clin. Neurophysiol.* 117, 348–368. doi:10.1016/j.clinph.2005.08.034.

Kayser, J., and Tenke, C. E. (2006b). Principal components analysis of Laplacian waveforms as a generic method for identifying ERP generator patterns: II. Adequacy of low-density estimates. *Clin. Neurophysiol.* 117, 369–380. doi:10.1016/j.clinph.2005.08.033.

Kristoufek, L. (2014). Measuring correlations between non-stationary series with DCCA coefficient. *Phys. A Stat. Mech. its Appl.* 402, 291–298. doi:10.1016/j.physa.2014.01.058.

Kwapień, J., Oświęcimka, P., and Drożdż, S. (2015). Detrended fluctuation analysis made flexible to detect range of cross-correlated fluctuations. *Phys. Rev. E* 92, 052815. doi:10.1103/PhysRevE.92.052815.

Lindquist, M. (2020). Neuroimaging results altered by varying analysis pipelines. *Nature* 582, 36–37. doi:10.1038/d41586-020-01282-z.

Makeig, S., Jung, T.-P., Bell, A. J., Ghahremani, D., and Sejnowski, T. J. (1997). Blind separation of auditory event-related brain responses into independent components. *Proc. Natl. Acad. Sci.* 94, 10979–10984. doi:10.1073/pnas.94.20.10979.

Mukli, P., Nagy, Z., Racz, F. S., Portoro, I., Hartmann, A., Stylianou, O., et al. (2021). Two-Tiered Response of Cardiorespiratory-Cerebrovascular Network to Orthostatic Challenge. *Front. Physiol.* 12. doi:10.3389/fphys.2021.622569.

Peng, C. K., Buldyrev, S. V, Havlin, S., Simons, M., Stanley, H. E., and Goldberger, A. L. (1994). Mosaic organization of DNA nucleotides. *Phys. Rev. E. Stat. Phys. Plasmas. Fluids. Relat. Interdiscip. Topics* 49, 1685–9. doi:10.1103/physreve.49.1685.

Perrin, F., Pernier, J., Bertrand, O., and Echallier, J. F. (1989). Spherical splines for scalp potential and current density mapping. *Electroencephalogr. Clin. Neurophysiol.* 72, 184–187. doi:10.1016/0013-4694(89)90180-6.

Podobnik, B., Jiang, Z.-Q., Zhou, W.-X., and Stanley, H. E. (2011). Statistical tests for power-law cross-correlated processes. *Phys. Rev. E* 84, 066118. doi:10.1103/PhysRevE.84.066118.

Podobnik, B., and Stanley, H. E. (2008). Detrended Cross-Correlation Analysis: A New Method for Analyzing Two Nonstationary Time Series. *Phys. Rev. Lett.* 100, 084102. doi:10.1103/PhysRevLett.100.084102.

Rubinov, M., and Sporns, O. (2010). Complex network measures of brain connectivity: Uses and interpretations. *Neuroimage* 52, 1059–1069. doi:10.1016/j.neuroimage.2009.10.003.

Stam, C. J., Nolte, G., and Daffertshofer, A. (2007). Phase lag index: Assessment of functional connectivity from multi channel EEG and MEG with diminished bias from common sources. *Hum. Brain Mapp.* 28, 1178–1193. doi:10.1002/hbm.20346.

Stam, C. J., and Van Dijk, B. W. (2002). Synchronization likelihood: An unbiased measure of generalized synchronization in multivariate data sets. *Phys. D Nonlinear Phenom.* 163, 236–251. doi:10.1016/S0167-2789(01)00386-4.

Steuer, R., Kurths, J., Daub, C. O., Weise, J., and Selbig, J. (2002). The mutual information: Detecting and evaluating dependencies between variables. *Bioinformatics* 18, S231–S240. doi:10.1093/bioinformatics/18.suppl_2.S231.

Stylianou, O., Racz, F. S., Eke, A., and Mukli, P. (2021a). Scale-Free Coupled Dynamics in Brain Networks Captured by Bivariate Focus-Based Multifractal Analysis. *Front. Physiol.* 11, 1–14. doi:10.3389/fphys.2020.615961.

Stylianou, O., Racz, F. S., Kim, K., Kaposzta, Z., Czoch, A., Yabluchanskiy, A., et al. (2021b). Multifractal Functional Connectivity Analysis of Electroencephalogram Reveals Reorganization of Brain Networks in a Visual Pattern Recognition Paradigm. *Front. Hum. Neurosci.* 15. doi:10.3389/fnhum.2021.740225.

van den Heuvel, M. P., and Fornito, A. (2014). Brain Networks in Schizophrenia. *Neuropsychol. Rev.* 24, 32–48. doi:10.1007/s11065-014-9248-7.

Zebende, G. F. (2011). DCCA cross-correlation coefficient: Quantifying level of cross-correlation. *Phys. A Stat. Mech. its Appl.* 390, 614–618. doi:10.1016/j.physa.2010.10.022.

Zhan, L., Jenkins, L. M., Wolfson, O. E., GadElkarim, J. J., Nocito, K., Thompson, P. M., et al. (2017). The significance of negative correlations in brain connectivity. *J. Comp. Neurol.* 525, 3251–3265. doi:10.1002/cne.24274.